RESEARCH ARTICLE | NOVEMBER 27 2023

Memristive devices with short-term and long-term memory behaviors for processing temporal information

Seung Jun Ki ; Jisoo Kim ; Mingze Chen ; Xiaogan Liang

Appl. Phys. Lett. 123, 223501 (2023)
https://doi.org/10.1063/5.0175200

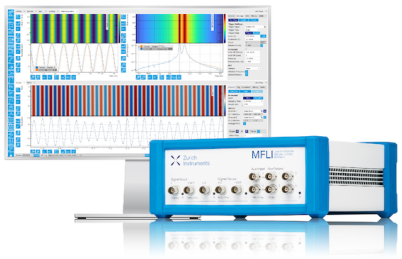

Applied Physics Letters ARTICLE pubs.aip.org/aip/apl

Memristive devices with short-term and long-term memory behaviors for processing temporal information

Cite as: Appl. Phys. Lett. **123**, 223501 (2023); doi: 10.1063/5.0175200
Submitted: 5 September 2023 · Accepted: 9 November 2023 ·
Published Online: 27 November 2023

Seung Jun Ki,[1] Jisoo Kim,[2] Mingze Chen,[1] and Xiaogan Liang[1,a)]

AFFILIATIONS

[1]Department of Mechanical Engineering, University of Michigan, Ann Arbor, Michigan 48109, USA
[2]Department of Electrical and Computer Engineering, University of Michigan, Ann Arbor, Michigan 48109, USA

[a)]Author to whom correspondence should be addressed: xiaoganl@umich.edu

ABSTRACT

Memristors based on 2D semiconductors such as MoS_2 and its derivative materials exhibit analog switching behaviors capable of emulating some synaptic functions, including short-term plasticity, long-term potentiation, and spike-time-dependent-plasticity. Additional investigation is needed to realize reliable control of such synaptic behaviors for practical device implementation. To meet this scientific need, we fabricated MoS_2-based memristors and studied their paired-pulse facilitation (PPF) and long-term memory characteristics under different pulse programming settings. This research has provided a guideline for identifying the programming settings for different neuromorphic processes. For example, a specific setting resulting in PPF $> 30\%$ and long-term conductance change $< 20\%$ has been identified to be suited for processing real-time temporal information. Furthermore, this research also indicates that the MoS_2 memristor keeps having an almost constant relative change in conductance but greatly enhanced drive current level under laser illumination. This behavior can enable an easy integration of such memristive devices with state-of-the-art controller circuits for practice neuromorphic control applications.

As the classical von-Neumann computing architecture approaches its performance ceiling, a variety of non-conventional devices are proposed for realizing neuromorphic circuits that could provide fast and energy-efficient in-memory computing.[1–3] Memristors are one of the promising candidates for this competition. The oxide-based filamentary memristors that feature discrete high and low resistance states (i.e., HRS and LRS) have been widely investigated, while a series of non-filamentary memristive devices based on layered materials have been also preliminarily studied and reported to exhibit several advantageous properties suitable for synaptic applications, such as high similitude with biological neuronal units, high degree of interconnectivity, and low threshold field magnitude for switching states.[4–7] Nevertheless, the current research activities on the 2D memristive devices mainly focus on the demonstration of proof-of-concept devices or implementation of 2D memristive devices under the state-of-the-art settings for operating filamentary memristors,[6,8–10] whereas the device society needs more research results about the unique properties of 2D memristive devices, especially the device physics knowledge for controlling and harvesting short-term and long-term memory behaviors of such devices. In addition, it is also highly desirable to develop device techniques that can enable easy integration of 2D memristive devices and realize practical neuromorphic computing functions beyond the static multiply accumulation (MAC) architecture.

Here, we present a systematic investigation on the short-term (ST) and long-term (LT) memory behaviors of MoS_2-based memristors and preliminarily explore the validity of utilizing such devices for rapid extraction of temporal information pieces from analog signals. Specifically, we study the effects of various pulse programming settings on the resultant pulse pair facilitation (PPF) values and LT conductance changes. These results and data establish a guideline for setting a MoS_2 memristor to ST or LT operation conditions for meeting different neuromorphic applications. In this work, we specifically demonstrate identification of the pulse programming setting suitable for processing real-time temporal information and implement it for processing analogue video scanline signals. Furthermore, this work also indicates that the instantaneous conductance and memristive modulation range of a MoS_2 memristor can be greatly enhanced under laser illumination. This result provides a convenient method for easing the integration of 2D semiconductor memristors with state-of-the-art circuits and realization of practical edge computing applications.

Figure 1 shows the optical micrograph (OM), zoomed scanning electron micrograph (SEM), and energy dispersive spectroscopy (EDS) mapping of an as-fabricated representative memristor with a multilayer MoS_2 channel sandwiched between a pair of interdigital metal electrodes (10 nm Ti/100 nm Au), which result in effective channel length of 800 nm and effective channel width of ~205 μm. The atomic force microscopy (AFM) characterization indicates that the average MoS_2 channel thickness is ~35 nm (Fig. S1 in the supplementary material). With such interdigital metal electrodes, the memristor device has a relatively short effective channel length and large effective channel width under a given footprint size of the device. Such a design can ensure a relatively high device conductance and ease the direct integration of such memristors with state-of-the-art circuit modules.

We first study the short-term (ST) memory behaviors of MoS_2 memristors. Specifically, the ST synaptic plasticity process involves rapid and reversible changes in the postsynaptic weight (represented by the device conductance) under the influence by presynaptic spikes.[11,12] This process is essential for generating spatial and temporal learning mechanisms.[13–15] PPF, a significant ST synaptic function, enables simple learning and information processing for temporary memory or computing tasks. Figure 2(a) illustrates the adjustable parameters of the programming pulses for emulating presynaptic neuron spikes and triggering postsynaptic PPF behaviors. These parameters include pulse width, interspike interval, and pulse amplitude. Figure 2(b) plots the PPF response signal curve (i.e., instantaneous postsynaptic current as the function of time) measured from a representative MoS_2 memristor. For this measurement, pulse width, interspike interval, and pulse amplitude are set to 5 ms, 5 ms, and 3 V, respectively. The resultant PPF ratio is calculated by using the following equation:

$$\text{PPF Ratio} = (A_2 - A_1)/A_1 \times 100\%, \tag{1}$$

where A_1 and A_2 are the excitatory postsynaptic currents induced by a pair of sequentially applied presynaptic spikes [or pulses, as illustrated by the dashed lines in Fig. 2(b)] with a specific interspike interval. Figure 2(c) plots the extracted PPF ratio data as the function of interspike intervals. For a MoS_2 memristor, the change in the synaptic response current caused by the second pulse is commonly higher than that induced by the first pulse, resulting in a PPF value > 0. In addition, with reduction of the interspike interval, the resultant PPF value rapidly increases.

Figure 3 displays the measured PPF values plotted as the functions of interspike intervals under different pulse programming settings. As depicted in Figs. 3(a) and 3(b), at a given interspike interval, the higher pulse amplitudes or the larger pulse widths result in the larger PPF values. Such observations are consistent with the ST synaptic characteristics observed in biological synapses.[16–18] They can be attributed to the previously reported scheme that the higher pulse amplitude or the longer pulse duration brings up the higher nonuniformity of the spatial distribution of S vacancies in the MoS_2 channel, therefore resulting in the larger plastic change in the instantaneous channel conductance.[6,19]

On the other hand, long-term (LT) synaptic plasticity is essential for the emulation of the nonvolatile changes of the synaptic weights and realization of the long-term learning ability of artificial neural networks. To investigate the LT potentiation behaviors of a MoS_2 memristor, we first measure its pulse-programmed characteristic curve that consists of a programming stage, during which a series of pulses are applied to the device and cause a progressive change of the device conductance represented by the instantaneous current measured under a sampling voltage of 1 V, and a subsequent relaxation stage, during which no more programming pulses are applied and the device exhibits a progressive recovery process of the conductance. Figure 4(a) shows the pulse-programmed characteristic curve measured from a representative device subjected to 2000 programming pulses (voltage: 5 V, pulse period: 2 ms, and duty cycle: 50%). The relaxation segment is fitted by an exponential decay function [Eq. (2)], where t is the lapsed time counted since the beginning of the relaxation process; τ_1 and τ_2 are the relaxation time constants of two main relaxation schemes associated with S vacancy diffusion and charge traps, respectively,[6,20,21] and C_1 and C_2 are the nominal magnitudes of these two relaxation effects, and I_{post} is the current representing the final device conductance after the programming course,

$$I = I_{post} + c_1 e^{-\frac{t}{\tau_1}} + c_2 e^{-\frac{t}{\tau_2}}. \tag{2}$$

In this work, the relative LT conductance change is calculated as

$$\text{LT Conductance Change} = (I_{post} - I_0)/I_0 \times 100\%, \tag{3}$$

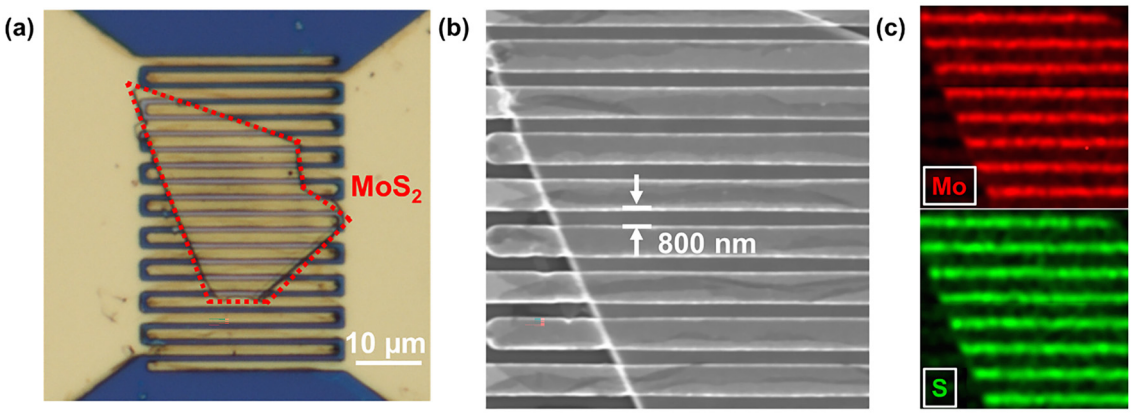

FIG. 1. (a) OM image, (b) zoomed SEM image, and (c) EDS elemental mapping image of an as-fabricated MoS_2 memristor with interdigital metal electrodes.

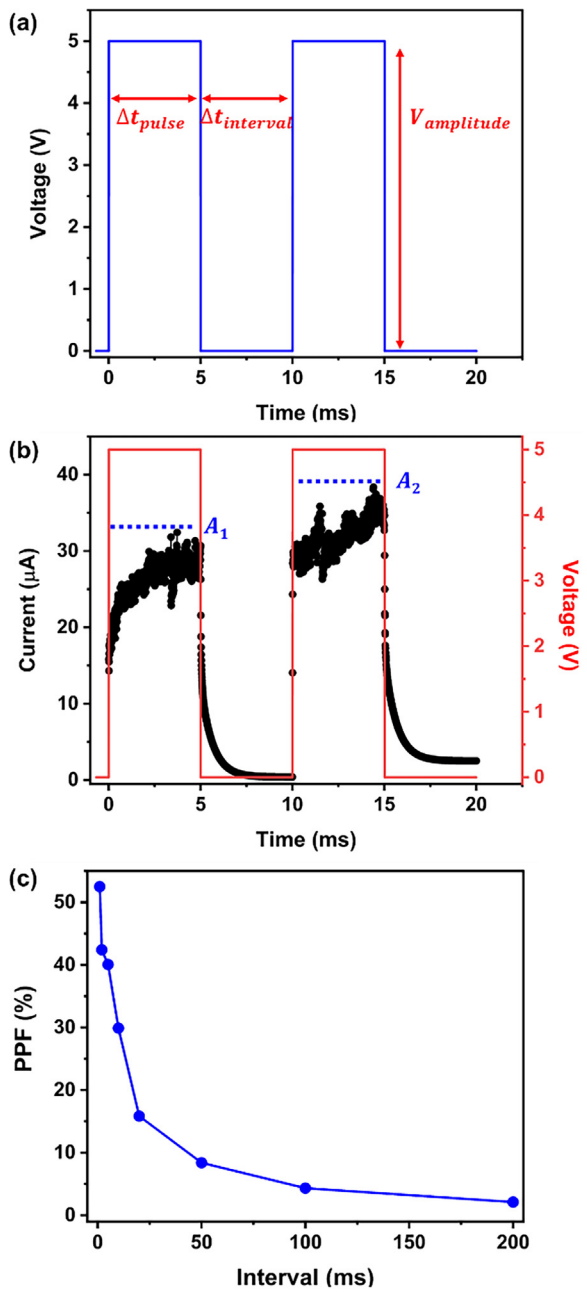

FIG. 2. (a) Illustration of a pair of programming voltage pulses (presynaptic spikes) with adjustable parameters of pulse amplitude ($V_{amplitude}$), pulse width (Δt_{pulse}), and interspike interval ($\Delta t_{interval}$); (b) PPF response (postsynaptic current) signal triggered by presynaptic spikes, which is measured from a presentative MoS_2 memristor; and (c) extracted PPF ratios plotted as the function of interspike intervals.

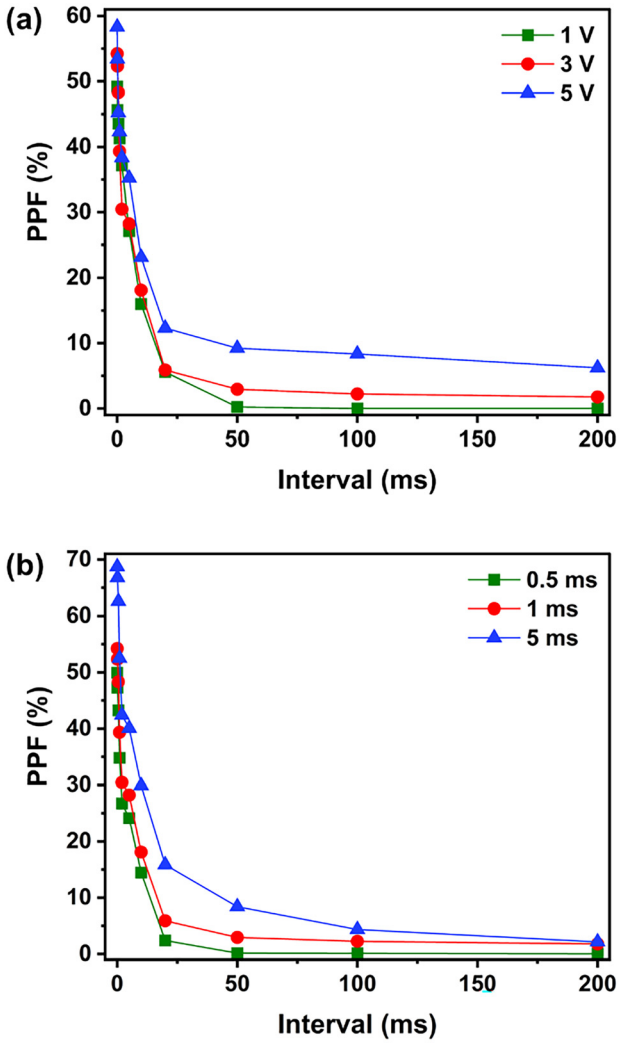

FIG. 3. PPF data plotted as the function of the interspike interval under different pulse programming settings: (a) fixed pulse width of 1 ms and different pulse amplitudes of 1, 3, and 5 V and (b) fixed pulse amplitude of 3 V and different pulse widths of 0.5, 1, and 5 ms.

where I_0 is the initial current value representing the initial device conductance before application of pulses. Such a LT conductance change is attributed to the field-induced accumulation of S vacancies around the electrodes, which is expected to result in the permanent changes in the Schottky barrier heights at MoS_2/metal interfaces as well as the whole device conductance.[6]

Figures 4(b)–4(d) display the extracted LT conductance change data plotted as the functions of pulse amplitudes (pulse duty cycle: 50%; pulse width: 1 ms; number of pulses: 2000), pulse duty cycles (pulse amplitude: 5 V; pulse width: 1 ms; number of pulses: 2000), and number of pulses (pulse amplitude: 5 V; pulse width: 0.5 ms; pulse duty cycle: 50%) (corresponding pulse-programmed characteristic curves are presented in Fig. S2 in the supplementary material). These results show that the LT conductance change becomes more prominent with increasing pulse amplitude, pulse duty cycle, or number of applied pulses. Specifically, the LT conductance change exhibits a quasi-linear dependence on pulse amplitude and pulse duty cycle, while it shows a parabolic-like dependence on the number of applied

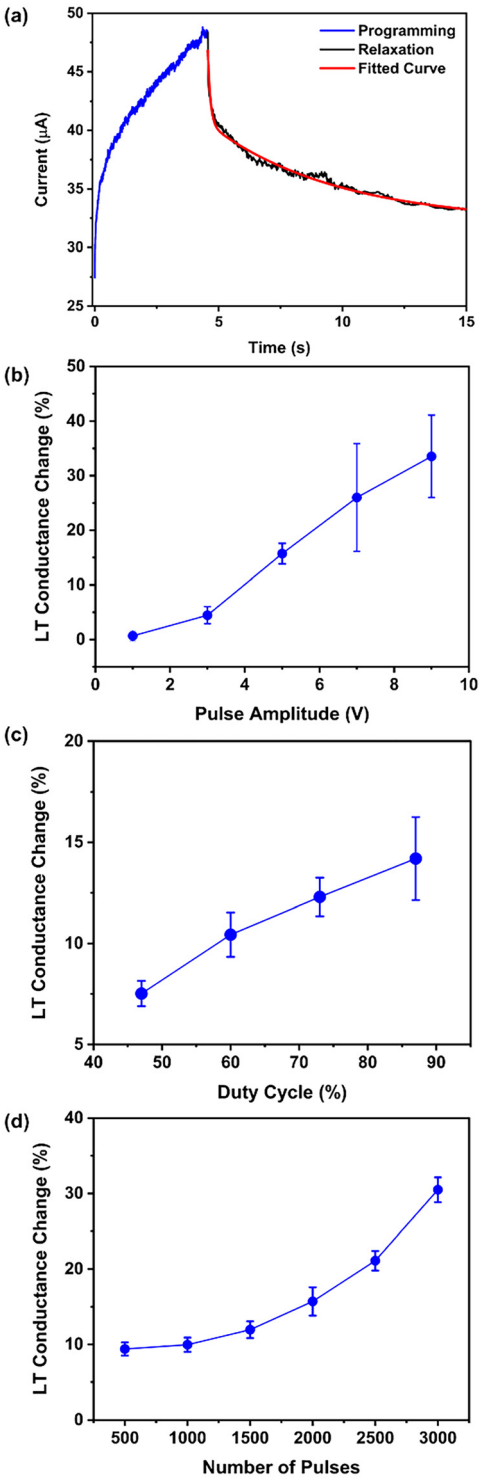

FIG. 4. (a) Pulse-programmed characteristic curve measured from a representative MoS_2 memristor in which the current sampled at 1 V represents the instantaneous device conductance; (b)–(d) the LT conductance changes as the function of pulse amplitudes, pulse duty cycles, and number of applied pulses, respectively.

pulses. This implies that increase in the number of applied pulses is a relatively more effective way to induce a large LT conductance change. The similar phenomena related to repeated-stimulation-induced ST-to-LT memory transitions have been reported by Wang *et al.*, Ohno *et al.*, and Chang *et al.*[22–24]

The aforementioned results highlight the influence of pulse programming settings on both ST and LT memory behaviors of MoS_2 memristors. Such data provide a guideline for configuring the pulse programming parameters to meet the requirements of specific neuromorphic applications. For instance, for extracting temporal information pieces from analog signals, the memristive device needs to be set to work in the ST memory regime, preferentially rendering a large PPF value and suppressed LT conductance change. A more practical requirement is that PPF $>$ 30% and LT conductance changes $<$ 20%. Based on our results, we can identify a suitable pulse programming setting for meeting this requirement, i.e., pulse amplitude of 5 V, duty cycle of ∼50%, pulse period of 1 ms, and number of applied pulses ∼500 per programming cycle (i.e., accumulative time for electrically stressing the device at 5 V is ∼250 ms per cycle). Figure 5(a) displays the response curve of a MoS2 memristor under such a programming setting. This device exhibits a prominent ST memory behavior as well as an analog conductance change behavior. To enable easy and direct integration of such memristors with current digital or analog circuits for realizing practical neuromorphic control applications, the output current from a MoS_2 memristor needs to be $>$ 0.1 mA at V = 3.3–5 V, whereas the current levels of our memristors biased at 5 V are typically less than 30 μA, as demonstrated in Fig. 5(a). In this work, we found that a convenient solution for this issue is to apply a continuous laser illumination to the memristor. As demonstrated in Fig. 5(b), under laser illumination (wavelength: 525 nm; power density: 5 mW/cm^2), the current level of the same MoS_2 memristor is boosted to the 0.1 mA level that can be easily sampled by a regular microcontroller unit (MCU) such as ATmega328, while the relative memristive change of the device conductance remains almost a constant.

Finally, the laser-illuminated MoS_2 memristor shown in Fig. 5(b) is used to preliminarily test the validity for extracting temporal information pieces from analog video stream signals without analog-to-digital signal conversion or software implementation. Figures S3 and S4 in the supplementary material illustrate the working scheme and circuit diagram of this test. Specifically, as illustrated in Fig. S3, the video stream signal from an analog camera on a lab-built robotic rover is fed to a MoS_2 memristor. Such an analog video signal is composed of time-sequential voltage scanlines. Each of the scanlines starts with a negative pulse and has a duration of ∼64 μs. When the camera captures the views of a bright vertical line against the dark background (i.e., a benchmarking object for this type of tests) from different distances, the resultant scanlines can be approximately regarded as voltage pulses with different duty cycles. Such pulse-like scanline signals, when properly amplified and applied to the memristor, are expected to dynamically modify the conductance of the memristor to different values. Such conductance values could be directly sensed by a regular MCU circuit for controlling the motorized wheels of the robotic rover. As illustrated in Fig. S4, the circuit of the aforementioned rover system specifically consists of an ATmega328-based microcontroller (Arduino UNO), a L298N motor driver, and an 800TVL NTSC analog camera. During the experimental process, the scanline signals from the camera are amplified by a LM358 amplifier to let the average amplitude of the

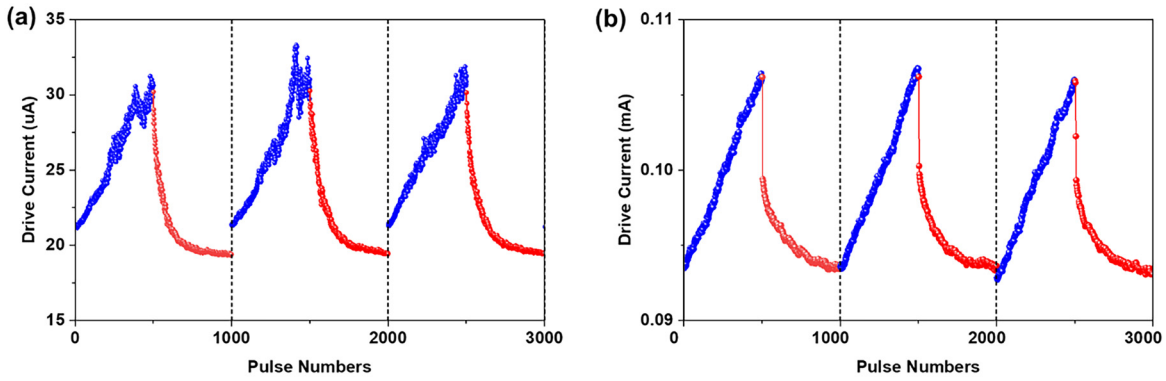

FIG. 5. Pulse-programmed characteristics of a MoS_2 memristor that is set to function as a short-term memory, measured under (a) dark condition and (b) laser illumination.

scanline pulses be ~5 V. When such amplified scanline signals are fed to the memristor, the resultant conductance signal (i.e., current signal at 5 V) in the MoS_2 channel is converted to a voltage signal using a current-to-voltage (I-to-V) converter and sampled by a 10-bit analog pin of the microcontroller. In this test, it has been demonstrated that the final MCU readings show a strong dependence on the perspective size (or the distance) of the bright line object. This device scheme could be further implemented for creating a collision avoidance system. Here, we present a supplemental video (Video S1) preliminarily showing that such MCU readings corresponding to the memristor's responses to analog video signals can be used to control the rover motors (a more detailed description of experimental condition and results is presented in the supplementary material). Moreover, a comparison table (Table S1) is included in the supplementary material, providing a quantitative evaluation of essential operational parameters, such as energy consumption per spike and PPF, for the presented device in comparison to state-of-the-art analog (or non-filamentary multi-state) memristive devices. In the future, multiple MoS_2 memristors could be implemented to construct the networks capable of rapidly extracting more complicated graphic information from analog video signals without analog-to-digital conversion.

In summary, this study presents a systematic study on the ST and LT memory behaviors of multilayer MoS_2 memristors, utilizing metrics such as PPF and LT conductance change. Our experimental results show that such memristors can be set to ST or LT memory regimes by adjusting pulse programming parameters, catering to specific application requirements. Moreover, we preliminarily demonstrated a neuromorphic system based on a photo-excited MoS_2 memristor integrated with an analog camera, which can enable direct extraction of temporal information pieces from analog video signals without analog-to-digital signal conversion or software implementation. This work has advanced knowledge for controlling the memristive response behaviors of 2D semiconductor memristors and provided technical insights for integrating such memristive devices with state-of-the-art controller circuits for practice neuromorphic control applications.

See the supplementary material for the AFM scanline of the MoS_2 channel (Fig. S1), pulse-programmed characteristic curves measured from a MoS_2 memristor under different pulse programming settings (Fig. S2), the schematic diagram of the experiment for demonstrating extraction of temporal information pieces from analog video signals using a MoS_2 memristor (Fig. S3), the circuit diagram of the experiment for demonstrating extraction of temporal information pieces from analog video signals using a MoS_2 memristor (Fig. S4), extraction of temporal information pieces from analog video signals and controlling of the motors on a robotic rover using a MoS_2 memristor (video S1), and a comparison chart of the memristor device working conditions (Table S1).

This work was supported by NSF under Grant No. CMMI-2001036. The authors would like to thank the staff of the University of Michigan's Lurie Nanofabrication Facility for providing the support of device fabrication and metrologies as well as Professor Wei D. Lu for help with access to the semiconductor parameter analyzer tools for memristors.

AUTHOR DECLARATIONS

Conflict of Interest

The authors have no conflicts to disclose.

Author Contributions

Seung Jun Ki: Conceptualization (lead); Data curation (equal); Visualization (equal); Writing – original draft (equal). **Jisoo Kim:** Data curation (supporting); Visualization (supporting); Writing – original draft (supporting). **Mingze Chen:** Data curation (supporting); Methodology (supporting); Validation (supporting). **Xiaogan Liang:** Conceptualization (lead); Funding acquisition (lead); Project administration (lead); Writing – original draft (equal); Writing – review & editing (lead).

DATA AVAILABILITY

The data that support the findings of this study are available from the corresponding author upon reasonable request.

REFERENCES

[1]S. Kumar, X. Wang, J. P. Strachan, Y. Yang, and W. D. Lu, Nat. Rev. Mater. **7**(7), 575 (2022).
[2]F. Cai, J. M. Correll, S. H. Lee, Y. Lim, V. Bothra, Z. Zhang, M. P. Flynn, and W. D. Lu, Nat. Electron. **2**(7), 290 (2019).
[3]A. Sebastian, M. Le Gallo, R. Khaddam-Aljameh, and E. Eleftheriou, Nat. Nanotechnol. **15**(7), 529 (2020).

[4]V. K. Sangwan and M. C. Hersam, Nat. Nanotechnol. **15**(7), 517 (2020).
[5]X. Zhu, D. Li, X. Liang, and W. D. Lu, Nat. Mater. **18**(2), 141 (2019).
[6]D. Li, B. Wu, X. Zhu, J. Wang, B. Ryu, W. D. Lu, W. Lu, and X. Liang, ACS Nano **12**(9), 9240 (2018).
[7]K. Zhu, X. Liang, B. Yuan, M. A. Villena, C. Wen, T. Wang, S. Chen, F. Hui, Y. Shi, and M. Lanza, ACS Appl. Mater. Interfaces **11**(41), 37999 (2019).
[8]P. Kumar, K. Zhu, X. Gao, S.-D. Wang, M. Lanza, and C. S. Thakur, npj 2D Mater. Appl. **6**(1), 8 (2022).
[9]W. Huh, D. Lee, and C.-H. Lee, Adv. Mater. **32**(51), 2002092 (2020).
[10]A. A. Bessonov, M. N. Kirikova, D. I. Petukhov, M. Allen, T. Ryhänen, and M. J. Bailey, Nat. Mater. **14**(2), 199 (2015).
[11]G.-Q. Bi and M.-M. Poo, J. Neurosci. **18**(24), 10464 (1998).
[12]G.-Q. Bi and M.-M. Poo, Nature **401**(6755), 792 (1999).
[13]D. V. Buonomano, J. Neurosci. **20**(3), 1129 (2000).
[14]K. Roy, A. Jaiswal, and P. Panda, Nature **575**(7784), 607 (2019).
[15]R. Gütig and H. Sompolinsky, Nat. Neurosci. **9**(3), 420 (2006).
[16]W. Xu, H. Cho, Y.-H. Kim, Y.-T. Kim, C. Wolf, C.-G. Park, and T.-W. Lee, Adv. Mater. **28**(28), 5916 (2016).
[17]R. Yang, H.-M. Huang, and X. Guo, Adv. Electron. Mater. **5**(9), 1900287 (2019).
[18]M.-K. Kim and J.-S. Lee, ACS Nano **12**(2), 1680 (2018).
[19]D. Li, B. Ryu, and X. Liang, Appl. Phys. Lett. **117**(21), 213102 (2020).
[20]M. Chen, Y. Wang, N. Shepherd, C. Huard, J. Zhou, L. J. Guo, W. Lu, and X. Liang, ACS Nano **11**(1), 1091 (2017).
[21]M. Chen, H. Rokni, W. Lu, and X. Liang, Microsyst. Nanoeng. **3**(1), 17053 (2017).
[22]Z. Q. Wang, H. Y. Xu, X. H. Li, H. Yu, Y. C. Liu, and X. J. Zhu, Adv. Funct. Mater. **22**(13), 2759 (2012).
[23]T. Ohno, T. Hasegawa, T. Tsuruoka, K. Terabe, J. K. Gimzewski, and M. Aono, Nat. Mater. **10**(8), 591 (2011).
[24]T. Chang, S.-H. Jo, and W. Lu, ACS Nano **5**(9), 7669 (2011).